Am J Transl Res 2024;16(10):5813-5828
www.ajtr.org /ISSN:1943-8141/AJTR0158930

Original Article

Polyphenol-enriched fraction from a Chinese herbal compound granule protects against D-galactose-induced apoptosis and metabolic disorders in PC12 cells

Zulifeiya Wusiman[1], Batuer Maimaitiming[1], Reziyanmu Yasen[1], Maiwulanijiang Yizibula[2]

[1]*Xinjiang Medical University College of Pharmacy, Urumqi 830017, Xinjiang, China;* [2]*Central Laboratory of Xinjiang Medical University, Urumqi 830011, Xinjiang, China*

Received July 3, 2024; Accepted September 28, 2024; Epub October 15, 2024; Published October 30, 2024

Abstract: Objectives: To investigate the protective effects of polyphenol-enriched fraction (PEF) derived from a Chinese herbal compound granule (HCG) against D-galactose (DG) induced injury in PC12 cells, and to analyze the metabolic pathways related to PC12 cell proliferation and apoptosis through a hydrogen-nuclear magnetic resonance (^{1}H-NMR) metabonomic study. Methods: The PEF was separated from HCG extraction and quantified by ultraviolet spectrophotometry following purification. DG-induced PC12 cells were treated with three different dosages of PEF. Cell vitality was assessed by the MTT method, cell counts were obtained after β-galactosidase staining, and cell apoptosis was detected by flow cytometry. Then, ^{1}H-NMR with partial least squares discrimination analysis (PLS-DA) and orthogonal partial least squares discrimination analysis (OPLS-DA) were performed to evaluate the intracellular metabolic profiles and pathways related to PC12 cell proliferation and apoptosis. Results: PEF significantly increased the PC12 cell survival rate, enhanced intracellular superoxide dismutase (SOD) activity, decreased malondialdehyde (MAD) levels, and inhibited both early and late apoptosis in response to DG-induced cytotoxicity. A total of 28 differential metabolites across 5 metabolic pathways, including phenylalanine, tyrosine and tryptophan biosynthesis, phenylalanine metabolism, glycine, serine and threonine metabolism, arginine biosynthesis, glyoxylate and dicarboxylate metabolism, were disturbed in PC12 cells. Conclusion: The protective effect of PEF is likely mediated via regulating and improving the down-regulated metabolic pathways, leading to suppressed oxidative stress and inhibited apoptosis.

Keywords: Polyphenol-enriched fraction, ^{1}H-NMR, apoptosis, metabolic pathway

Introduction

Globally, the aging population is gradually growing, and aging-related neurodegenerative disorders significantly impact the health and quality of life of elderly. This issue has attracted global attention [1]. The morphological structures and physiological functioning of different cells, organs, and tissues slowly degrade as people age, which is a delicate and complex natural physiological occurrence [2]. Aging leads to decline in the functions of multiple organs and systems, especially brain activity. Meanwhile, aging is a major risk factor for the development of Parkinson's disease (PD), Alzheimer's disease (AD), Huntington's disease, cancer, and others [3], resulting in high mental pressure on patients and substantial economic burden on families and society [4, 5].

While the mechanisms of aging are complex, they can be explained by several theories, including the well-accepted free radical theory [6]. According to the "free radical theory of aging", cellular damage caused by free radicals, particularly reactive oxygen species (ROS), contributes to the aging process [7]. Clinical investigations have also shown that patients with various neurodegenerative illnesses, such as aging, AD, and PD, exhibit significantly elevated ROS levels in their brain tissues [8-10].

Animals often use D-galactokinase and galactose-1-phosphate uridyltransferase to metabo-

https://doi.org/10.62347/EGNA1218

Table 1. Constituents of the herbal compound granule (HCG)

Botanical name	Family	Chinese name	Part used	Ratio (%)	Voucher no.
Adiantum capillus veneris L.	Adiantaceae	Tie-xian-jue	Herb	13.3	Y160214
Glycyrrhiza uralensis Fisch.	Fabaceae	Gan-cao-gen	Radix or rhizome	20.0	Y150709
Ficus carica Linn.	Moraceae	Wu-hua-guo	Dried Fruit	20.0	Y170425
Foeniculum vulgare Mill.	Umbelliferae	Xiao-hui-xiang	Fruit	13.3	Y141206
Red Vitis vinifera L.	Vitaceae	Pu-tao	Dried Fruit	13.3	Y130623
Rosa rugosa Thunb.	Rosa	Mei-gui-hua	Dried petal	6.7	Y150154
Pimpinella Anisum L.	Umbelliferae	Yang-hui-xiang	Fruit	13.3	Y140546

lize the reducing sugar D-galactose (DG) [11]. However, when the accumulation of DG exceeds the catalytic ability of these two enzymes, aldose reductase converts the excessive DG into galactitol, which is non-digestible and accumulates in the cell, leading to osmotic stress and the production of ROS [12]. The human body maintains a dynamic equilibrium between the production and elimination of free radicals. Excessive accumulation of free radicals can damage cells and macromolecules, leading to age-related degenerative diseases [13, 14]. Therefore, DG-induced oxidative stress in mice has been utilized as both an *in vivo* model to investigate aging and AD, and also an *in vitro* model with rat pheochromocytoma 12 (PC12) cells [15]. Although derived from a transplantable rat pheochromocytoma, the PC12 cell line is valuable in neuroscience research, particularly in studies of neurotoxicity and neuroprotection [16].

Metabolomics adds information to genomes and proteomics. ^{1}H-NMR spectroscopy and mass spectrometry have facilitated the practical application of metabolomics to several scientific fields, enabling comprehensive analysis on the spectroscopic fingerprints of biofluids, plants, cells, and tissues [17]. Cell culture metabolomics focuses on the cell as a unit, enabling precise analysis of intracellular and extracellular metabolic profiles at the cellular level. This approach has been applied in many areas, including cellular physiology, cell differentiation process, diseases pathogenesis, viral infections, and foodomics [18].

HCG is a traditional herbal remedy composed of seven medicinal plants, including *Adiantum capillus veneris L., Glycyrrhiza uralensis Fisch., Ficus carica Linn., Foeniculum vulgare Mill., Vitis vinifera L., Rosa rugosa Thunb., and Pimpinella anisum L.* As a traditional folk medicine in northwest China, HCG has been used to treat various age-related disorders, including memory impairment and behavioral symptoms associated with dementia. Previous study showed that HCG could ameliorate cognitive dysfunction and enhance learning and memory abilities in DG-induced aging model mice [19]. Moreover, our prior cell metabonomic study indicated that the total phenols and flavonoids extracted from HCG could induce apoptosis of SiHa, HeLa, and C-33A cervical cancer cells in vitro, while inhibiting their proliferation by regulating altered pathways in energy, amino acid, lipid, and nucleic acid metabolisms [20]. In this study, PEF was isolated from HCG extraction and quantified by ultraviolet spectrophotometry after purification. DG was subsequently used to establish a PC12 oxidative stress model to evaluate the possible neuroprotective effects. During investigating possible mechanisms, the effects of total polyphenols on intracellular metabolic profiles of PC12 cells were measured by the ^{1}H-NMR method with PLS-DA and OPLS-DA analysis. Subsequently, network analysis was employed to explore the associated metabolic pathways influenced by differential metabolites related to cell proliferation and apoptosis in DG-stimulated PC12 cells.

Materials and methods

Material

All plant materials were sourced from the Xinjiang Uighur Autonomous Region Traditional Uighur Medicine Hospital in Urumqi, China. The components of HCG are shown in **Table 1**. PC12 cells were purchased from iCell Bioscience Inc. (Shanghai, China), derived from transplantable male rat adrenal pheochromocytoma-differentiated strains. The PC12 cell line expresses a receptor for nerve growth factor (NGF), which induces a neurophenotype.

Fetal bovine serum (FBS) and Dulbecco's modified eagle medium (DMEM, 0022619) were acquired from Biological Industries Company (Israel). Antibiotics (Penicillin and Streptomycin) (040902), phosphate buffered saline (PBS), 0.25% trypsin, annexin V-PE apoptosis test kit for 7-AAD were purchased from TransGen Biotech (Beijing, China). Gallic acid standard (110831-201605) was purchased from National Institutes for Food and Drug Control (Beijing, China). Methyl thiazolyl tetrazolium (MTT, EZ3412B205) was purchased from Saiguo Biotech (Goungzhou, China). 30-60 mesh polyamide (20121022) was purchased from Biochemical Plastics Factory (Zhejiang, China). Cell cycle and apoptosis kit (120919-200526) and cell senescence β-galactosidase staining kit (122019200413) were purchased from Biyuntian Biotech (Shanghai, China). 0.05% sodium 3-trimethlysilyl [2,2,3,3-2H4] propionate acid and D-galactose (WXBD12-91V) was provided by Sigma Aldrich Inc. (St. Louis, MO, USA). Commercial kits for superoxide dismutase (SOD, 20200713), lactic dehydrogenase (LDH, 20200710), and malondialdehyde (MDA, 20200704) were acquired from Jiancheng Bioengineering Institute (Nanjing, China). Analytical-grade $NaH_2PO_4 \cdot 12H_2O$ and $Na_2HPO_4 \cdot 2H_2O$ were bought from Guoyao Chemical Co., Ltd. (Shanghai, China).

Preparation and content determination of PEF in HCG

HCG powder (3 Kg) was soaked in 30 L of double-distilled water (ddH_2O) at 80°C for 12 h, followed by heating to 105 ± 5°C for 2 h. The resulting extract was centrifuged (5000×g for 15 min at 4°C) and then filtered through a 0.2-μm filter. The extract was then subjected to vacuum drying at 60 ± 5°C, yielding a fine spray-dry extract at a rate of 17.4% (w/w). Next, 250 g of 30-60 mesh polyamide was activated by 95% ethanol and packed into a column. 400 g of the dried extract was dissolved in three times its volume of water (60°C), stirred for 0.5 h and centrifuged at 3000 rpm for 15 minutes (Thermo Scientific KS12 centrifuge). The supernatant was then passed through the prepared 30-60 mesh polyamide column at 1.0 mL/min for adsorption and stood for 2 h after complete adsorption. After that, the column was subsequently eluted with water until colorless, followed by three rounds of elution with 60% ethanol, each using three times the volume of ethanol. All 60% ethanol eluents were then collected and processed into a dry polyphenol-rich fraction, achieving a yield of 17.78% (w/w).

The total polyphenol content of PEF was measured using the Folin-Ciocalteu (FC) test as previously described [21]. Briefly, 10 mL of gallic acid was used to prepare standard solutions (70, 60, 50, 40, 30, and 0 μg/ml), and PEF samples (20 μg/ml) were mixed with 1 mL of FC reagent. 1.5 mL of sodium carbonate (Na_2CO_3) at a concentration of 20% (w/v) was then added to the mixture, which was left at room temperature for 2 h. Finally, the absorbance was measured at 765 nm using an ultraviolet spectrophotometer (UV-2550PC, Simadzu, Japan). The observed total phenol content in PEF was 30.83%.

Cell culture and treatment

The PC12 cells were cultured in DMEM supplemented with 10% fetal bovine serum (FBS) and 1% antibiotics (1000 units/ml penicillin and 1000 units/ml streptomycin) in a humidified incubator with 5% CO_2 and 95% air at 37°C. The cells were harvested at 90% confluence. Cell survival rate was measured by trypan blue assay, with survival rates exceeding 95%. PEF and DG were fully dissolved in DMEM under ultrasonic conditions and then diluted with culture medium. PC12 cells were treated with PEF at final concentrations of 3.75, 7.5, and 15 μg/mL for 24 h. Following this, 16 mg/mL of DG was added to each well, and the cells were incubated for an additional 48 h.

MTT assay

MTT was used to evaluate cell viability as previously described [22]. PC12 cells were seeded into 96-well plates and incubated for 24 h. Then, the cells were treated with PEF at final concentrations of 3.75, 7.5, and 15 μg/mL. After 24 h incubation, each well was supplemented with 16 mg/mL DG, and the cells were further incubated for 48 h. Subsequently, 10 μL of 5 mg/mL MTT solution was added to each well. Following a 4-h incubation at 37°C, the supernatant was aspirated with a pipette, and 100 mL of DMSO was added. The absorbance was measured at 490 nm with a microplate reader (Multiskan GO, Thermo, USA).

Staining for senescence-associated β-galactosidase (SA-β-Gal)

In vitro senescence was assessed by measuring SA-β-Gal activity using a staining kit according to the manufacturer's instruction [23]. The stained cells were observed using a fluorescence microscope (BA120, Leica, Germany) connected to a digital camera. The number of SA-β-Gal-positive and -negative cells in each complete image was quantified using Image Pro-Plus 6.0 software (Olympus, Tokyo, Japan). The percentage of SA-β-Gal positive cells was computed for analysis.

Flow cytometry

Flow cytometry was performed as described previously [24]. After the specified procedure, PC12 cells were suspended in trypsin without EDTA. The PC12 cells were then collected by centrifugation at 4°C and 1000 rpm for 5 minutes. Following resuspension in 1× binding buffer, the cells were treated with 5 μL annexin V-PE and 5 μL 7-AAD for 15 minutes at room temperature in the absence of light. Samples were analyzed using a flow cytometer (BDLSRII, BD Biosciences, USA) within 1 h of staining.

Determination of MDA, SOD, and LDH contents in PC12 cells

PC12 cells were seeded into 24-well plates and incubated for 24 h before being treated with PEF at final concentrations of 3.75, 7.5, and 15 g/mL. After 24 h, DG (16 mg/mL) was added to each well followed with another 48 h culture. Cells were harvested and centrifuged at 4°C for 10 minutes (12000 g). The LDH level in cell supernatants was determined using an ELISA kit (Jiancheng Bioengineering Institute, Nanjing, China) as directed. Furthermore, the collected PC12 cells were lysed on ice, and the resulting lysates were centrifuged (12000 g, 10 min) at 4°C. The supernatants were collected for SOD and MDA analysis using ELISA kits (Jiancheng Bioengineering Institute, Nanjing, China) according to the manufacturer's instructions.

Analysis of metabolomics

The sample collection and metabolite extraction procedures used in this investigation were adapted from previously reported procedures with slight modification [25]. Briefly, PC12 cells that pretreated with various concentrations of PEF (3.75, 7.5, or 15 μg/mL) for 24 h were seeded at 5×10^4 cells/flask in 200 cm^2 cell culture flasks and subjected to DG (16 g/L) stimulation for 48 h. At approximately 100% confluency, the cells were harvested using trypsin solution, counted, and 5.0×10^7 cells were collected. The cells were quenched in liquid nitrogen, washed with PBS, and stored at -80°C. Pellets were suspended in 1 mL of ice-cold 1:2 (v/v) water/methanol solution, subjected to three freeze-thaw cycles, to extract the intracellular metabolites. The pellets were then sonicated in an ice water bath for 15 minutes followed with centrifugation at 12000 rpm for 10 minutes at 4°C. The supernatant was collected in a 5 mL Eppendorf tube. The remaining pellets were extracted again using the same procedures. The pooled supernatants were lyophilized and stored at -80°C. For further NMR investigation, cell extraction samples (n = 5) were gathered.

The dried cell extracts were diluted in 600 L of sodium 3-trimethylsilyl-1-[2, 2, 3, 3-2H4] propionate (TSP)-containing D2O phosphate buffer (0.1 M Na_2HPO_4/NaH_2PO_4, pH = 7.4). The dissolved solution was kept at room temperature for 10 min and then centrifuged at 10000 rpm at 4°C for 10 min. The clear supernatant (550 μL) was transferred into a 5-mm NMR tube (Wilmad Lab, Glass, USA) for spectroscopic analysis. The ^{1}H-NMR spectra of each sample were recorded using the NOESYPRESAT-ID pulse sequence on a Varian Unity Inova 600 NMR spectrometer (Varian 600, USA), operating at a proton frequency of 599.95 MHz. A total 128 scans were acquired per sample over 32768 data points with a spectral width of 10000 Hz, resulting in an acquisition time of 1.64 seconds and a relaxation delay of 2 seconds at 298 kHz. Two-dimensional NMR was performed on selected samples for assignment purposes, in addition to the ^{1}H-^{1}H homonuclear correlation spectroscopy (COSY) test, the total correlation spectroscopy (TOCSY) test, and the J-resolved (J-Res) test.

MestReNova (Mestrelab Research, Santiago de Compostela, Spain, version 5.2.5) was used to phase all spectra and correct the baseline. The TSP chemical shift was calibrated at δ0.00 ppm. To appropriately reflect the integrated bucket intensities to the integrated peak areas,

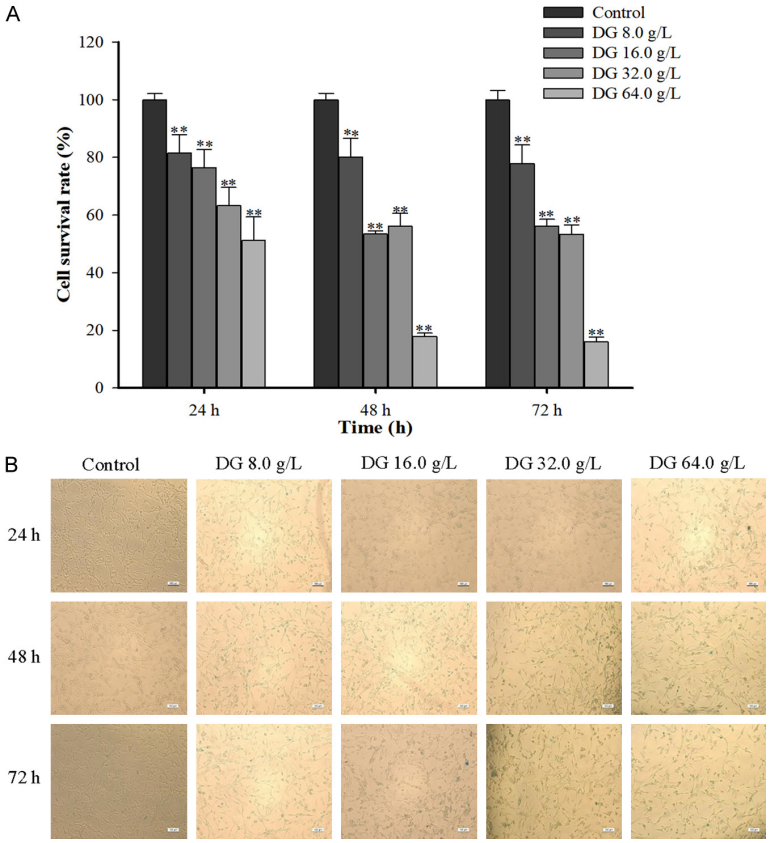

Figure 1. D-Galactose induced PC12 cell damage. A. PC12 cell viability after being stimulated with different concentrations of D-Galactose for 24 h, 48 h, and 72 h, respectively. B. Effects of D-Galactose on cellular senescence of PC12 cells (×100). All data were expressed as mean ± SD (n = 6). $^{**}P < 0.01$ *vs*. the control.

the spectra were binned into δ0.003 ppm wide buckets from δ0.00 to δ9.00 ppm. The bucket width was adjusted to match the width of the resonances at the base of the peaks. The regions with δH = 5.22-4.68 ppm were excluded from the analysis due to the high variability in water intensity. Each bin's area was then normalized to the entire spectrum area. Multivariate data analysis was performed on the normalized data using SIMCA-P version 14.1 software (Umetrics, Umea, Sweden). Validation of the model was carried out using PLS-DA, and sample separation was maximized using OPLS-DA. In an OPLS-DA model, the orthogonal signal correction filter was integrated into the partial least-squares regression method. The X matrix is NMR data. Using one partial least-squares and one orthogonal component, the class information for the various groups as the Y variables was determined [26]. The parameters R2X and Q2 in this study were used to describe the quality of OPLS-DA model. The X matrix's total explained variation was represented by R2X. Q2 showed a connection between the model's statistical validity and predictability.

Network analysis

MetaboAnalyst 5 (http://www.metaboanalyst.ca/MetaboAnalyst) was used to analyze the metabolic pathways affected by significant differential metabolites ($P < 0.05$) following PEF treatment in DG-damaged PC12 cells. The significance of each pathway was assessed based on effect size and pathway enrichment analysis, with values greater than 0.1 considered indicative of the most significant pathways in response to DG stimulation.

Statistical analysis

SPSS 17.0 (SPSS, Inc.) was used for statistical analyses. Data were expressed as mean ± standard deviation. One-way ANOVA followed with Tukey's post hoc test was used for multiple group comparisons. $P < 0.05$ was deemed statistically significant.

Results

DG induced PC12 cell damage

PC12 cell viability (**Figure 1A**) and cellular senescence (**Figure 1B**) were tested by MTT assay and SA-β-Gal staining. DG treatment (0, 8, 16, 32, and 64 mg/mL) significantly affected PC12 cell viability and induced cellular senescence. Specifically, exposure to DG at 64 mg/mL resulted in less than 20% cell viability after 48 and 72 hours, while treatment with 16 and 32 mg/mL increased viability to 50-60% during the same timeframe. Notably, 8 mg/mL of DG maintained cell viability at around 80% across all time points. In addition, there was a time- and dose-dependent increasing trend in the

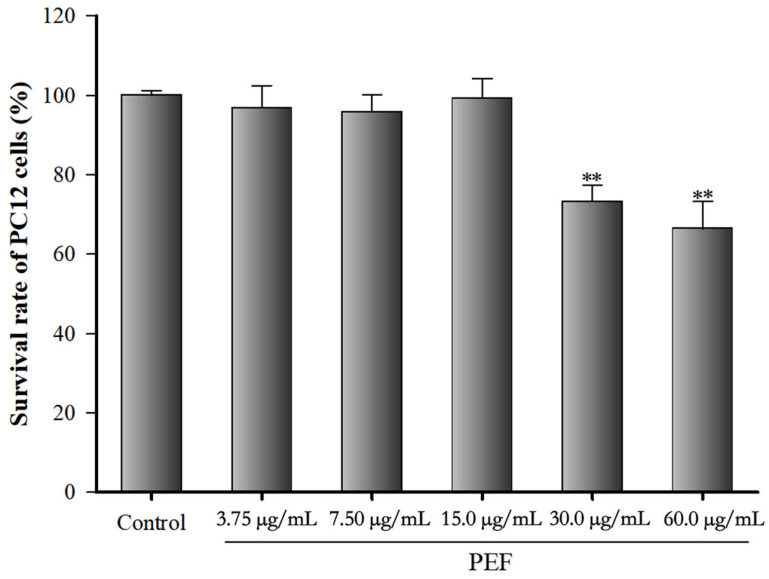

Figure 2. Effect of polyphenol-enriched fraction on PC12 cell viability. PC12 cells were treated with 0, 3.75, 7.5, 15, 30, and 60 μg/mL of polyphenol-enriched fraction for 24 h. All data were expressed as mean ± SD (n = 6). $^{**}P < 0.01$ *vs*. the control.

positive staining rate of PC12 senescent cells in the SA-β-Gal staining test. Collectively, 16 mg/mL of DG stimulation for 48 h was chosen as the optimal condition to induce cytotoxicity in PC12 senescent cells for this study (n = 6).

Effect of PEF on PC12 cell viability

PC12 cell viability was tested by MTT assay (**Figure 2**). Cells were treated with 0, 3.75, 7.5, 15, 30, and 60 μg/mL of PEF for 24 h. Compared with normal control PC12 cells, the cell viability was significantly reduced by 73% and 66% after the treatment with PEF at 30 and 60 μg/mL for 24 h (all $P < 0.01$). No significant differences in cell viability (97%, 96%, 99%) were observed after the treatment with lower concentration of PEF (3.75, 7.5, and 15 μg/mL) for 24 h ($P > 0.05$). This suggests that 3.75, 7.5, and 15 μg/mL are appropriate concentrations for PEF treatment, while 30 and 60 μg/mL of PEF can lead to severe cytotoxicity.

PEF protected against DG-induced cytotoxicity in PC12 cells

Figure 3A shows the effects of PEF on cell viability of DG-injured PC12 cells. Compared to the control group, cell viability of DG-injured PC12 cells was significantly reduced by 57% ($P < 0.01$). However, PEF pre-treatment significantly increased PC12 cell viability by 92%, 71%, and 67% at the concentrations of 3.75, 7.5, and 15 μg/mL, respectively (all $P < 0.01$).

Figure 3B, **3C** show the effects of PEF on cell senescence after stimulation of DG-injured PC12 cells. Compared to the control group, DG treatment significantly increased the positive staining rate of senescent cells by 54% ($P < 0.01$); however, PEF-pretreated cells demonstrated substantially lower senescence rates at 8%, 13%, and 12% corresponding to the PEF concentrations of 3.75, 7.5, and 15 μg/mL, respectively, which were significantly lower than the rate in DG-treated cells (all $P < 0.01$).

As shown in **Figure 3D**, the LDH level increased by 97.51% in DG-injured PC12 cells ($P < 0.01$) compared to the control group. However, pretreatment with 3.75, 7.5, and 15 μg/mL PEF significantly reduced LDH leakage by 37.74%.

PEF inhibited DG-induced apoptosis in PC12 cells

Flow cytometry results revealed that DG exposure significantly increased both early and late cell apoptosis in PC12 cells (all $P < 0.01$). Nevertheless, PEF pretreatment significantly decreased cell apoptosis induced by DG ($P < 0.01$) (**Figure 4A-C**).

PEF suppressed DG-induced oxidative stress in PC12 cells

DG-injured PC12 cells exhibited elevated MDA level compared to the control group ($P < 0.01$). In contrast, PEF pretreatment markedly reduced MDA level (**Figure 5A**, $P < 0.01$). Additionally, DG exposure significantly decreased the SOD levels in PC12 cells, and PEF pretreatment significantly restored the lev-

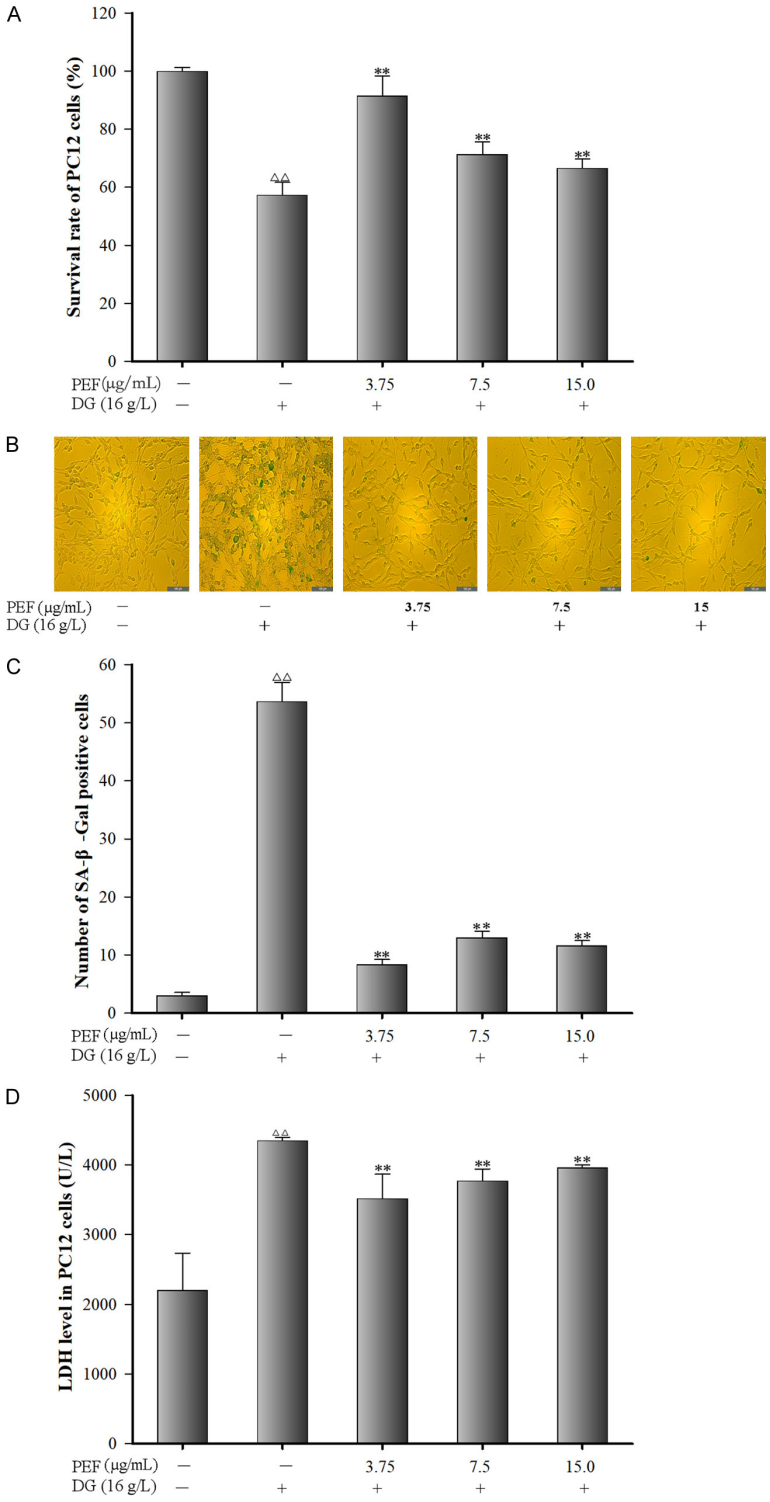

Figure 3. Effects of polyphenol-enriched fraction on D-Galactose induced cytotoxicity in PC12 cells. A. Effect of polyphenol-Enriched fraction on cell viability in D-Galactose-induced PC12 cells (n = 6); B. SA-β-Gal positive staining images of PC12 cells (×100); C. SA-β-Gal positive staining rate of PC12 cells (n = 3); D. Effects of polyphenol-enriched fraction on lactate dehydrogenase leakage in D-Galactose-induced PC12 cells. All data were expressed as mean ± SD (n = 6). $^{\Delta\Delta}P < 0.01$ *vs*. the control; $^{**}P < 0.01$ *vs*. the model group.

els of SOD in DG-injured PC12 cells (**Figure 5B**, $P < 0.01$).

^{1}H-NMR spectra of PC12 cells and metabolites pattern analysis

The typical ^{1}H-NMR spectrum of PC12 cells across all groups is shown in **Figure 6**. PLS-DA analysis of the integral values obtained from the spectra is presented in a 3D spatial distribution plot, indicating a model prediction reliability (R^2Y = 0.311, Q^2 = 0.194). Different colors were used to represent different groups, with each dot representing a single sample. As shown in **Figure 7**, the distribution areas for each group are basically well separated. In addition, the spatial distribution of PC12 cells in each group was relatively independent from the other groups, indicating that their metabolic profiles differ significantly.

The OPLS-DA method was further used to analyze the differential metabolic compounds between the two groups. The results, displayed in the score plots and corresponding S-plots (**Figure 8**), show changes in the intensity of some metabolite signals in the intracellular extracts of PC12 cells following DG stimulation and PEF treatment. Metabolites with $P < 0.05$ and VIP value ≥ 1.0 were considered differential (**Table 2**). A total of 28 distinguishable metabolites were identified, showing dynamic metabonomic responses to PEF treatment in DG-stimulated PC12 cells (**Figure 6**).

According to our preliminary data, compared with the con-

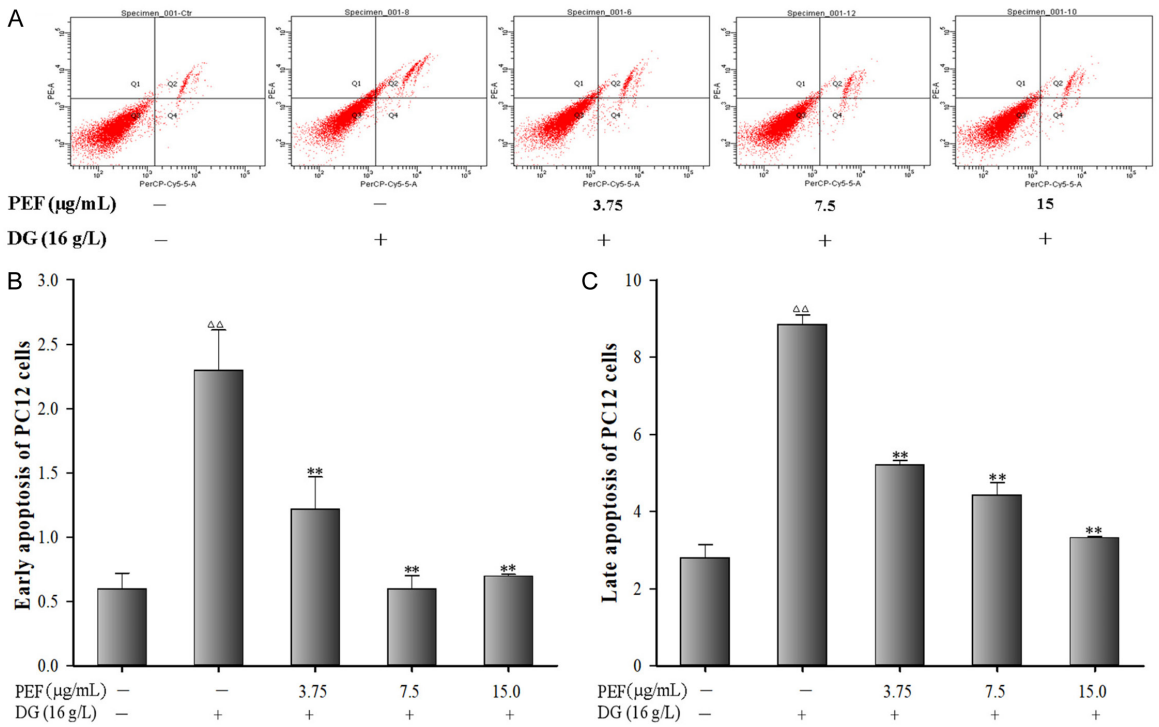

Figure 4. Effects of polyphenol-enriched fraction on D-Galactose-induced apoptosis in PC12 cells. A. Apoptosis of PC12 cells; B. Early apoptosis in PC12 cells; C. Late apoptosis in PC12 cells. All data were expressed as mean ± SD (n = 3). $^{\Delta\Delta}P < 0.01$ *vs*. the control; $^{**}P < 0.01$ *vs*. the model group.

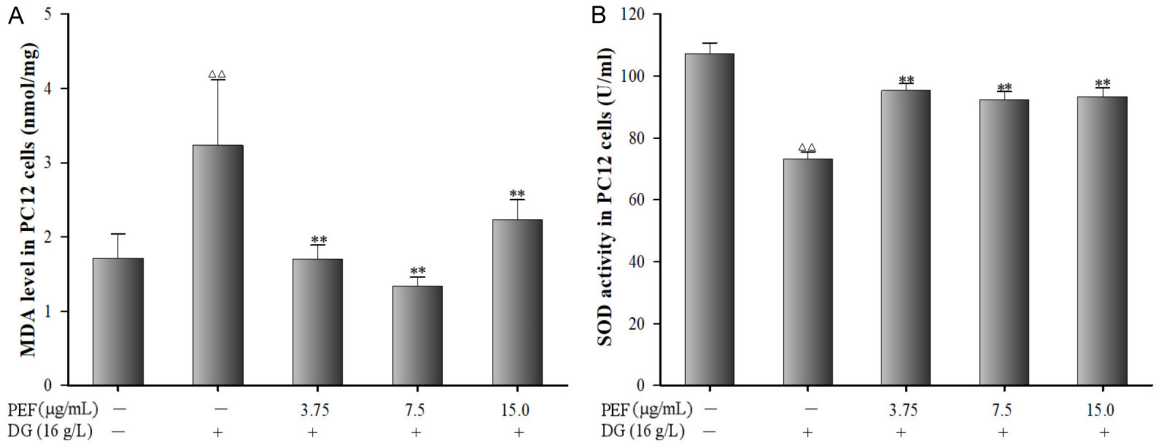

Figure 5. Effects of polyphenol-enriched fraction on D-Galactose-induced oxidative stress in PC12 cells. A. Malondialdehyde level in PC12 cells. B. Superoxide dismutase activity in PC12 cells. All data were expressed as mean ± SD (n = 6). $^{\Delta\Delta}P < 0.01$ *vs*. the control; $^{**}P < 0.01$ *vs*. the model group.

trol group, intracellular extracts from DG-stimulate PC12 cells exhibited reduced levels of amino acids, including isoleucine, leucine, alanine, valine, lysine, glycine, proline, citrulline, threonine, tyrosine, and phenylalanine. Other metabolites, including lactic acid, acetic acid, glutamine, carnitine, α-ketoglutaric acid, creatine, choline, taurine, scyllitol, inositol, glutathione, adenosine phosphate, 6,8-dihydroxypurine, inosine, and formic acid, might also play an important role in metabolic changes. Besides, higher levels of α-glucose, β-glucose, and glutathione were also observed. Many of these metabolites displayed distinct patterns in the PEF pretreated groups, especially in 7.5 μg/mL group.

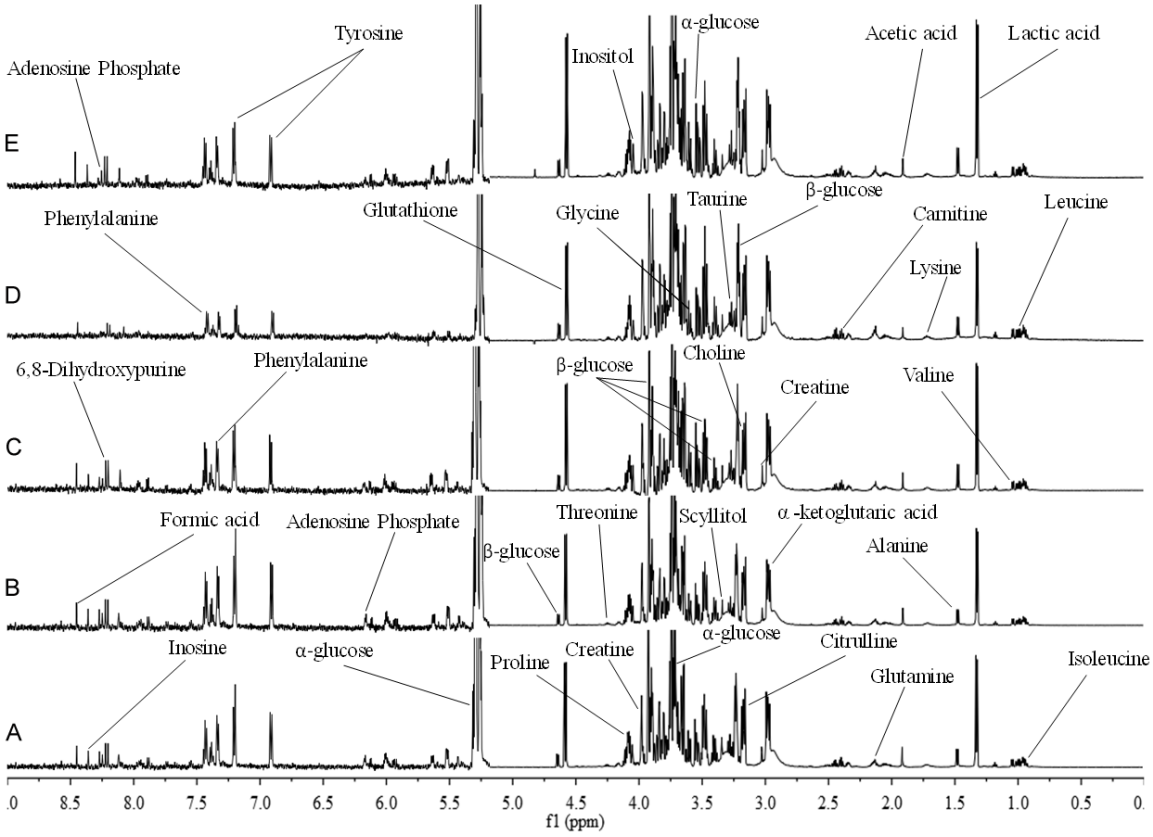

Figure 6. Typical ^{1}H NMR spectra (600 MHz) of intracellular extracts of PC12 cells. The δ9.0-5.3 ppm region was expanded 6 times compared to the δ5.3-0.0 ppm region. A. Control group. B. D-Galactose (16.0 mg/mL) treatment group. C. D-Galactose (16.0 mg/mL) + polyphenol-enriched fraction (3.75 μg/mL) group. D. D-Galactose (16.0 mg/mL) + polyphenol-enriched fraction (7.5 μg/mL) group. E. D-Galactose (16.0 mg/mL) + polyphenol-enriched fraction (15.0 μg/mL) group.

Analysis of metabolic pathways

The differential metabolites identified through ^{1}H-NMR metabonomic analysis underwent further investigations to identify the most significantly interrupted pathways via MetaboAnlyst 5.0 online analysis platform (http://www.metaboanalyst.ca) and KEGG Database analysis (http://www.genome.jp/kegg/). The results, displayed in **Table 3**, highlight key metabolic pathways with impact values greater than 0.10 and *p*-values less than 0.05. The impact value at the X-axis represents the relevance index of each metabolic pathway, as determined by topological analysis, while the significance of pathway enrichment is shown by -log(P) on the Y-axis. As both the impact value and -log(P) increase, the size of the corresponding circles also increases, indicating stronger correlations between the metabolic differences observed across groups (**Figure 9**).

Discussion

Aging is currently understood as a process driven by the accumulation of various cellular and molecular damages over time, including altered DNA and damaged protein molecules [27]. According to the World Health Organization, the global population of older adults (60 years and older) reached 900 million in 2015 and is projected to increase to two billion by 2050. This not only presents significant challenges to global economy and society but also escalates the risk of neurodegenerative disorders, strokes, and cancer [28]. Considering the rapidly increasing aging global population and the severity of aging-related severe disorders, the search for effective anti-aging agents is now one of the most pressing challenges in biomedical research.

One of the main contributors to senescence is oxidative stress, which leads to DNA and cyto-

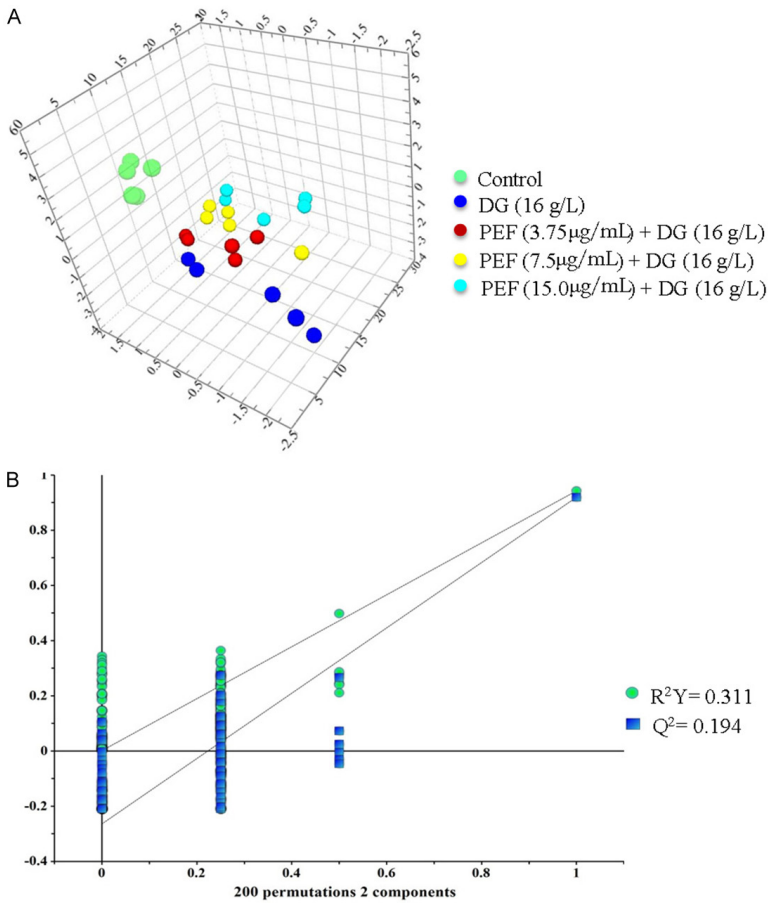

Figure 7. Partial least squares discrimination analysis of PC12 cells pretreated with polyphenol-enriched fraction (3.75, 7.5, and 15 μg/mL) followed by D-Galactose stimulation. A. Results of three-dimensional spatial distribution plot. B. Model validation result of partial least squares discrimination analysis.

membrane damage, deficits in proteins and enzyme metabolism, as well as reactive oxygen species (ROS)-induced cellular apoptosis [29, 30]. The levels of these oxidative stressors gradually increase over the lifespan. When it outweighs the body's repair capacity, this damage affects multiple systems, impair mitochondrial function, halts cellular differentiation (particularly the central nervous system), and speed up the aging process [31]. Accumulated oxidative stress may be one of the primary processes underlying cognitive aging and neurodegenerative disorders, including Parkinson's disease (PD) and Alzheimer's disease (AD) [32].

PC12 cells, a commonly used neuronal cell line, are widely used in the *in vitro* studies of nervous system diseases [33]. Increasing evidence suggests that DG-induced neuronal cell death is primarily caused by apoptosis [34, 35]. In this study, DG-stimulated PC12 cells showed a 57% reduction in viability, while PEF pretreatment (3.75, 7.5, and 15 μg/mL) protected against DG-induced cytotoxicity, with cell viability increased by 92%, 71%, and 67%, respectively. Results of SA-β-Gal senescence marker staining indicated that PEF pretreatment (3.75, 7.5, and 15 μg/mL) significantly inhibited the positive staining rates of PC12 cells. In addition, after cell damage, cell membrane permeability increased, leading to intracellular LDH release into the supernatant after centrifugation. PEF pretreatment (3.75, 7.5, and 15 μg/mL) significantly reduced LDH leakage by 37.74%, 26.25%, and 17.67%, respectively. The above results indicate that PEF has promising effects on protecting PC12 cells from DG-induced cell damage and cytotoxicity. The protective effect of PFF on DG-induced cell injuries appears dose-dependent. While PFF shows potential as a neuroprotective agent against brain senescence, the optimal drug concentration range needs further exploration.

Apoptosis plays a crucial role in aging by maintaining the homeostatic balance between cell formation and cell death in tissues. It acts as a defensive mechanism, triggered when cells are damaged by noxious agents or diseases [36]. The mitochondrial and death receptor pathways are two main pathways implicated in apoptosis [37]. In this research, the effect of PEF on DG-induced PC12 cell apoptosis was verified. The results illustrated that PEF pretreatment could significantly decrease both the early and late cell apoptosis induced by DG (16 mg/mL) exposure. Meanwhile, DG exposure raised the cellular MDA levels and reduced the SOD enzyme activity, while PEF significantly inhibited the rise in MDA levels and restored SOD activity, suggesting that the protective

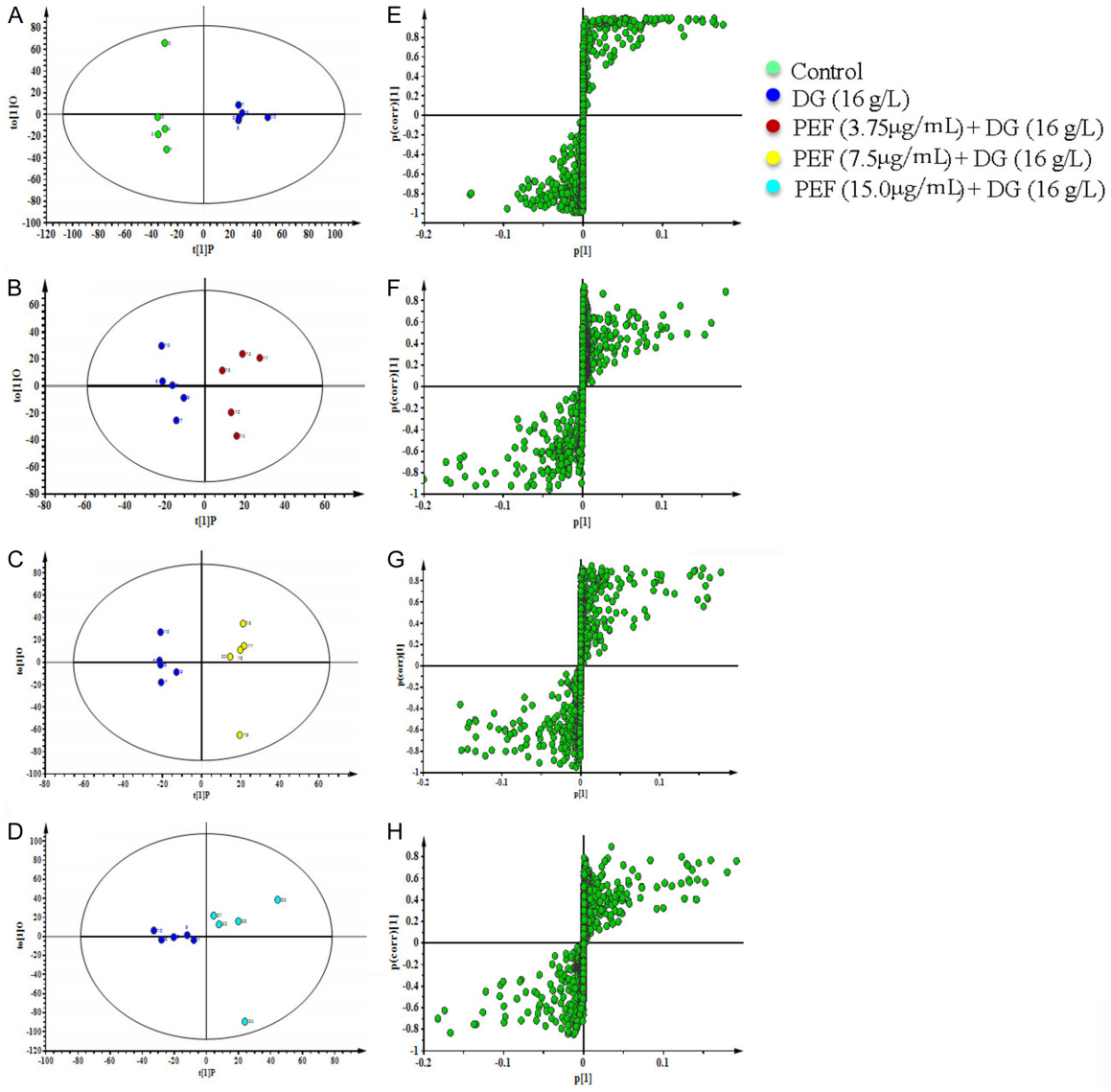

Figure 8. Plots of each group's orthogonal partial least squares discrimination analysis scores and related S-plots. A, E. Orthogonal partial least squares discrimination analysis score plot and S-plot of control group versus the D-Galactose (16.0 mg/mL) group. B, F. Orthogonal partial least squares discrimination analysis score plot and S-plot of D-Galactose (16.0 mg/mL) group versus D-Galactose (16.0 mg/mL) + polyphenol-enriched fraction (3.75 μg/mL) group. C, G. Orthogonal partial least squares discrimination Analysis score plot and S-plot of D-Galactose (16.0 mg/mL) group versus D-Galactose (16.0 mg/mL) + polyphenol-enriched fraction (7.5 μg/mL) group. D, H. Orthogonal partial least squares discrimination analysis score plot and S-plot of DG (16.0 mg/mL) group versus D-Galactose (16.0 mg/mL) + polyphenol-enriched fraction (15.0 μg/mL) group.

effect of PEF against DG-induced PC12 cell damage and apoptosis may be due to its antioxidant potential. These findings are consistent with previous *in vitro* studies, which reported that Chinese herbal compound granula could improve the memory and learning ability in a DG-induced aging model in mice [19].

In addition, ^{1}H NMR metabonomics analysis, MetaboAnlyst 5.0 online analysis, and KEGG Database-based metabolic pathway analysis identified 28 differential metabolites related to amino acid and carbohydrate metabolism as part of the metabolite profile of DG-injured PC12 cells. In this study, 5 key disturbed metabolic pathways were identified, including path-

Table 2. The differentially expressed metabolites in each group

No	Metabolites	Chemical shift (ppm)	Control *vs* DG		DG *vs* DG+PEF-L		DG *vs* DG+PEF-M		DG *vs* DG+PEF-H	
			P-value	VIP-value	*P*-value	VIP-value	*P*-value	VIP-value	*P*-value	VIP-value
1	Isoleucine	0.93 (t), 1.00 (d)	-0.027623	1.4802	0.0354487	1.79214	0.0343171	1.82082	0.032644	1.66577
2	Leucine	0.95 (d), 0.97 (d)	-0.0291702	1.5445	0.0345913	1.68896	0.0257759	1.3677	0.0345913	1.68896
3	Valine	0.98 (d), 1.04 (d)	-0.0283861	1.5014	0.0356528	1.74547	0.026198	1.39056	0.0321493	1.36776
4	Lactic acid	1.33 (d), 4.11 (q)	-0.0272466	1.42377	0.0302286	1.3405	0.0316459	1.67988	0.0347051	1.3427
5	Alanine	1.47 (d)	-0.0251632	1.3181	0.0263205	1.30948			0.03179	1.09124
6	Lysine	1.71 (m), 3.76 (m)	-0.0292181	1.53725	0.03437	1.83168	0.0291676	1.54879	0.03437	1.83168
7	Acetic acid	1.92 (s)	-0.0238886	1.26624			-0.0334	1.77318		
8	Proline	2.05 (m), 2.34 (m), 4.18 (t)	-0.0246604	1.32488	0.0268576	1.05077	0.0373108	1.97745	0.0277299	1.04836
9	Glutamine	2.13 (m), 3.76 (m)	-0.0255533	1.36665	0.0338737	1.4887	0.0347435	1.84195	0.0305272	1.4047
10	Carnitine	2.46 (dd)	-0.0230596	1.25878	0.0395386	2.09668	0.0389602	2.06707	0.0271679	1.3223
11	α-ketoglutaric acid	2.98 (t)	-0.0273165	1.4421	0.024121	1.01794	0.0265727	1.4106	0.024121	1.01794
12	Creatine	3.03 (s), 3.93 (s)	-0.0243744	1.31344			0.0324652	1.72326		
13	Choline	3.21 (s)	-0.0226601	1.17397					0.0201827	1.5633
14	Taurine	3.27 (t), 3.43 (t)	-0.0252991	1.32989			0.0259196	1.3748	-0.0354015	2.02096
15	Scyllitol	3.35 (s)	-0.0285257	1.54139			-0.0348705	1.85196	-0.0197281	1.35114
16	Glycine	3.55 (s), 3.60 (d)	-0.0280687	1.45882	-0.0217581	1.44637	0.032433	1.72333	-0.0277605	1.64131
17	Citrulline	3.17 (m), 3.76 (t)	-0.0245912	1.28324	0.0257683	1.63336	0.0333103	1.76886	0.0256553	1.41304
18	α-glucose	3.53 (dd), 3.72 (dd), 5.23 (d)	0.028327	1.4673	0.0172667	1.3172	-0.0318631	1.69254	-0.0254691	1.16638
19	β-glucose	3.24 (dd), 3.40 (t), 3.47(ddd), 3.90(dd), 4.65 (d)	0.0276381	1.51945	0.0244507	1.42809	-0.0287331	1.52816	-0.0322455	1.3525
20	Inositol	4.06 (t)	-0.022362	1.13828			-0.034811	1.84839		
21	Threonine	4.25 (t)	-0.0250869	1.31106	0.0288714	1.17074	0.0345607	1.83426	0.0288714	1.17074
22	Glutathione	4.58 (d)	0.0222117	1.15066	-0.0255761	1.30109	0.0258243	1.37213	0.0254646	1.33512
23	Adenosine Phosphate	6.15 (d), 8.26 (s)	-0.0227684	1.21958	0.0340675	1.37766				
24	Tyrosine	6.89 (d), 7.19 (d)	-0.0265138	1.41294			0.0284928	1.51299		
25	Phenylalanine	7.32 (d), 7.42 (m)	-0.0287492	1.51563			0.0258294	1.37317		
26	6,8-Dihydroxypurine	8.20 (s)	-0.02364	1.21206			0.0278896	1.4803	-0.0219772	1.39832
27	Inosine	8.35 (s)	-0.023266	1.20194			0.027102	1.438		
28	Formic acid	8.45 (s)	-0.0245353	1.34999			0.0305163	1.61878		

Notes: To determine the *p* value, one-way ANOVA and Tukey's post hoc test for group comparisons were utilized. DG (16.0 mg/mL); PEF-L (3.75 μg/mL); PEF-M (7.5 μg/mL); PEF-H (15.0 μg/mL); d, doublet; m, multiplets; q, quartet; s, singlet; t, triplet; DG, D-Galactose; PEF, polyphenol-enriched fraction.

Table 3. Differential metabolite-related metabolic pathways by KEGG pathway analysis

No.	Pathway	Hits/Total	-log(*P*)	Raw *P*	Impact	FDR
1	Phenylalanine, tyrosine and tryptophan biosynthesis	2/4	2.8080	1.56E-03	1.0000	0.0327
2	Phenylalanine metabolism	2/12	1.8020	1.57E-02	0.3571	0.1893
3	Glycine, serine and threonine metabolism	4/34	2.7077	1.96E-03	0.2953	0.0329
4	Arginine biosynthesis	2/14	1.6713	2.13E-02	0.2284	0.2238
5	Glyoxylate and dicarboxylate metabolism	4/32	2.8083	1.55E-03	0.1058	0.0327

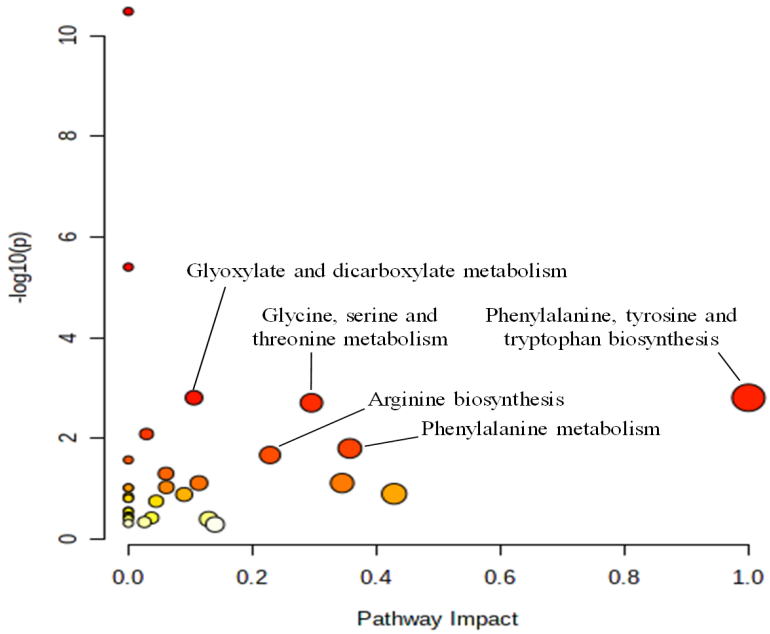

Figure 9. MetaboAnalyst pathway analysis results. The alterations to the metabolic pathways are shown as dots. The impact value at the X-axis denotes the relevance index of the metabolic route as determined by topological analysis, and the significance level of the enrichment study of metabolic pathways is represented by -log(P) at the Y-axis.

ways associated with phenylalanine metabolism, phenylalanine, tyrosine, and tryptophan biosynthesis, serine and threonine metabolism, glycine, arginine biosynthesis, glyoxylate, and dicarboxylate metabolism.

The amino acids tyrosine and phenylalanine are essential for production of monoamine neurotransmitters, which play a significant role in the development of neurodegenerative illnesses [38]. Phenylalanine, an essential amino acid, is primarily metabolized by its conversion to tyrosine via phenylalanine hydroxylase [39]. Tyrosine serves as a precursor to the catecholamine neurotransmitters dopamine and norepinephrine, which are involved in the brain's response to acute stresses by facilitating nerve signal transmission [40]. The primary cause of neurotoxicity and many neurological disorders like aging and AD is the disturbances in nerve signaling transmission [41]. In this study, the intracellular levels of tyrosine and phenylalanine were down-regulated in DG-injured PC12 cells. However, pretreatment with 7.5 μg/mL PEF significantly increased the contents of tyrosine and phenylalanine. Pathway analysis revealed that the biosynthesis of tyrosine, phenylalanine, and tryptophan, along with phenylalanine metabolism, were the most affected pathways in both DG exposure and PEF pretreatment groups. These results suggest that PEF could protect PC12 cells from DG-induced disturbance via regulation of pathways involved in nerve signal transmission and neurotransmitter formation.

Several neurodegenerative diseases and important metabolic pathways involved in cell signaling have all been linked to disrupted amino acid metabolism [42]. Clinical research revealed that one of the most significant pathways affected in frontotemporal dementia is glycine, serine, and threonine metabolism [43]. Defects in glycine and serine metabolism have also been associated with seizures in children [44]. Some *in vitro* studies also found that the metabolic pathway of glycine, serine, and threonine metabolism was perturbed in PC12 cells after corticosterone induction [38]. In the current study, disturbance of these metabolic pathways in DG-injured PC12 cells was observed, consistent with the above-mentioned findings.

Arginine is a crucial component for NO synthesis, synaptic plasticity, learning, and memory [44]. During the early phases of neurodegenerative diseases like AD, synthetic NO performs a

compensatory function in facilitating synaptic transmission [45]. Arginine is synthesized from glutamate through several enzymatic steps [46]. The present study indicated that DG exposure significantly reduced glutamate content of PC12 cells, further downregulating arginine biosynthesis. In contrast, PEF could significantly increase the glutamate content and improve the downregulated arginine biosynthesis in PC12 cells.

Furthermore, the current study revealed that energy metabolism pathways, including glyoxylate and dicarboxylate metabolism, were significantly decreased in DG-injured cells. This was confirmed by the abnormal decrease in α-ketoglutaric acid content and increase in α-glucose and β-glucose in PC12 cells. Interestingly, PEF significantly restored energy metabolism by inhibiting the downregulation of glyoxylate and dicarboxylate metabolism and maintaining a stable immune environment to inhibit the DG-induced PC12 cell damage and apoptosis.

Besides, our study illustrated that the content of proline and creatine in DG-induced PC12 cells was significantly decreased. It has been reported that as the sole proteinogenic amino acid, proline provides structural stability to proteins, serves as a key component for molecular recognition and signaling, and plays a role in learning and memory [47]. Reduced proline endopeptidase activity has been reported to be related to neuronal death and plaque formation in neurodegenerative diseases such as AD [48]. Furthermore, proline-rich polypeptides have been suggested as potential therapeutic agents for neurodegenerative diseases [49]. Creatine, involved in cellular metabolism through ATP supplementation, serves as an energy source that can be either endogenously synthesized or exogenously derived [50]. Previous reports showed that the supplementation of creatine exerted a significant neuroprotective effect in mouse models of neurodegenerative diseases, possibly due to its antioxidant and anti-apoptotic properties [51]. In this study, PEF treatment significantly increased the content of proline and creatine, which may be one of the possible mechanisms by which PEF protects PC12 cells against DG-induced cell damage and cytotoxicity.

Conclusion

PEF protects against DG-induced cytotoxicity in PC12 cells by suppressing oxidative stress and inhibiting apoptosis. Metabolomic studies revealed that 28 differential metabolites associated with five metabolic pathways were regulated by PEF, including phenylalanine, tyrosine, and tryptophan biosynthesis, phenylalanine metabolism, glycine, serine, and threonine metabolism, arginine biosynthesis, glyoxylate, and dicarboxylate metabolism. Therefore, PEF is a potential treatment for aging-related memory and learning impairments, though more clinical research is required.

Acknowledgements

This study was supported by the Natural Science Foundation Special Training Program of Xinjiang Uygur Autonomous Regional (2023-D03013) and PhD Research Startup Foundation of Xinjiang Medical University (XJMUYJ-20210604).

Disclosure of conflict of interest

None.

Address correspondence to: Maiwulanijiang Yizibula, Central Laboratory of Xinjiang Medical University, No. 393 Xinyi Road, Urumqi 830011, Xinjiang, China. Tel: +86-0991-2110325; E-mail: mawlanjan624@xjmu.edu.cn

References

[1] Huang J, Hou B, Zhang S, Wang M, Lu X, Wang Q and Liu Y. The protective effect of adiponectin-transfected endothelial progenitor cells on cognitive function in d-galactose-induced aging rats. Neural Plast 2020; 2020: 1273198.

[2] Andrade B, Jara-Gutiérrez C, Paz-Araos M, Vázquez MC, Díaz P and Murgas P. The relationship between reactive oxygen species and the cGAS/STING signaling pathway in the inflammaging process. Int J Mol Sci 2022; 23: 15182.

[3] Wang L, Du J, Zhao F, Chen Z, Chang J, Qin F, Wang Z, Wang F, Chen X and Chen N. Trillium tschonoskii maxim saponin mitigates D-galactose-induced brain aging of rats through rescuing dysfunctional autophagy mediated by Rheb-mTOR signal pathway. Biomed Pharmacother 2018; 98: 516-522.

[4] Ridderinkhof KR and Krugers HJ. Horizons in human aging neuroscience: from normal neu-

ral aging to mental (Fr)agility. Front Hum Neurosci 2022; 16: 815759.
[5] Yin P, Wu J, Wang L, Luo C, Ouyang L, Tang X, Liu J, Liu Y, Qi J, Zhou M and Lai T. The burden of COPD in China and its provinces: findings from the global burden of disease study 2019. Front Public Health 2022; 10: 859499.
[6] Jomova K, Raptova R, Alomar SY, Alwasel SH, Nepovimova E, Kuca K and Valko M. Reactive oxygen species, toxicity, oxidative stress, and antioxidants: chronic diseases and aging. Arch Toxicol 2023; 97: 2499-2574.
[7] Zhang JJ, Liu X, Pan JH, Zhao Q, Li YM, Gao WG and Zhang ZS. Anti-aging effect of brown black wolfberry on Drosophila melanogaster and d-galactose-induced aging mice. J Funct Foods 2020; 65: 103724.
[8] Iakovou E and Kourti M. A comprehensive overview of the complex role of oxidative stress in aging, the contributing environmental stressors and emerging antioxidant therapeutic interventions. Front Aging Neurosci 2022; 14: 827900.
[9] Moulton MJ, Barish S, Ralhan I, Chang J, Goodman LD, Harland JG, Marcogliese PC, Johansson JO, Ioannou MS and Bellen HJ. Neuronal ROS-induced glial lipid droplet formation is altered by loss of Alzheimer's disease-associated genes. Proc Natl Acad Sci U S A 2021; 118: e2112095118.
[10] Xiao B, Kuruvilla J and Tan EK. Mitophagy and reactive oxygen species interplay in Parkinson's disease. NPJ Parkinson Dis 2022; 8: 135.
[11] Kandeda AK, Nguedia D, Ayissi ER, Kouamouo J and Dimo T. *Ziziphus jujuba* (Rhamnaceae) alleviates working memory impairment and restores neurochemical alterations in the prefrontal cortex of D-galactose-treated rats. Evid Based Complement Alternat Med 2021; 2021: 6610864.
[12] Hu WS, Liao WY, Chang CH and Chen TS. Paracrine IGF-1 activates SOD2 expression and regulates ROS/p53 axis in the treatment of cardiac damage in D-galactose-induced aging rats after receiving mesenchymal stem cells. J Clin Med 2022; 11: 4419.
[13] Jomova K, Raptova R, Alomar SY, Alwasel SH, Nepovimova E, Kuca K and Valko M. Reactive oxygen species, toxicity, oxidative stress, and antioxidants: chronic diseases and aging. Arch Toxicol 2023; 97: 2499-2574.
[14] Kushwah N, Bora K, Maurya M, Pavlovich MC and Chen J. Oxidative stress and antioxidants in age-related macular degeneration. Antioxidants (Basel) 2023; 12: 1379.
[15] Hua X, Lei M, Zhang Y, Ding J, Han Q, Hu G and Xiao M. Long-term D-galactose injection combined with ovariectomy serves as a new rodent model for Alzheimer's disease. Life Sci 2007; 80: 1897-905.
[16] Wiatrak B, Kubis-Kubiak A, Piwowar A and Barg E. PC12 cell line: cell types, coating of culture vessels, differentiation and other culture conditions. Cells 2020; 9: 958.
[17] Paternain L and Campion J. Metabolomics and transcriptomics of metabolic disorders. Curr Nutr Rep 2013; 2: 199-206.
[18] Tian JS, Liu SB, He XY, Xiang H, Chen JL, Gao Y, Zhou YZ and Qin XM. Metabolomics studies on corticosterone-induced PC12 cells: a strategy for evaluating an in vitro depression model and revealing the metabolic regulation mechanism. Neurotoxicol Teratol 2018; 69: 27-38.
[19] Nueramina·Abuduhalike and Batur·Maimaitiming. Anti-aging effects of Chinese herbal compound granules on D-galactose-induced aging mice. Xinjiang Medical University 2023.
[20] Dinala·Qiarefuhan and Batur·Maimaitiming. Study the effects of total phenols and flavonoids in compound capillus-veneris granules on cervical cancer cells based on cell metabonomics. Xinjiang Medical University 2022.
[21] Wang YP, Wat E, Koon CM, Wong CW, Cheung DW, Leung PC, Zhao QS, Fung KP and Lau CB. The beneficial potential of polyphenol-enriched fraction from Erigerontis Herba on metabolic syndrome. J Ethnopharmacol 2016; 187: 94-103.
[22] Gao L, Zhou F, Wang KX, Zhou YZ, Du GH and Qin XM. Baicalein protects PC12 cells from $A\beta_{25\text{-}35}$-induced cytotoxicity via inhibition of apoptosis and metabolic disorders. Life Sci 2020; 248: 117471.
[23] Zhang W, Zhang Y, Hou J, Xu T, Yin W, Xiong W, Lu W, Zheng H, Chen J and Yuan J. Tris (2-chloroethyl) phosphate induces senescence-like phenotype of hepatocytes via the $p21^{Waf1/Cip1}$-Rb pathway in a p53-independent manner. Environ Toxicol Pharmacol 2017; 56: 68-75.
[24] Bi A, Guo Z, Yang G, Huang Y, Yin Z and Luo L. γ-glutamylcysteine suppresses cadmium-induced apoptosis in PC12 cells via regulating oxidative stress. Toxicology 2022; 465: 153029.
[25] Tian JS, Liu SB, He XY, Xiang H, Chen JL, Gao Y, Zhou YZ and Qin XM. Metabolomics studies on corticosterone-induced PC12 cells: a strategy for evaluating an in vitro depression model and revealing the metabolic regulation mechanism. Neurotoxicol Teratol 2018; 69: 27-38.
[26] Nijiati Y, Shan L, Yang T, Yizibula M and Aikemu A. A ^{1}H NMR spectroscopic metabolomic study of the protective effects of irbesartan in a rat model of chronic mountain sickness. J Pharm Biomed Anal 2021; 204: 114235.
[27] Hemagirri M and Sasidharan S. In vitro antiaging activity of polyphenol rich Polyalthia longi-

folia (Annonaceae) leaf extract in Saccharomyces cerevisiae BY611 yeast cells. J Ethnopharmacol 2022; 290: 115110.
[28] Barbagallo M, Veronese N and Dominguez LJ. Magnesium in aging, health and diseases. Nutrients 2021; 13: 463.
[29] Rybka J, Kupczyk D, Kędziora-Kornatowska K, Pawluk H, Czuczejko J, Szewczyk-Golec K, Kozakiewicz M, Antonioli M, Carvalho LA and Kędziora J. Age-related changes in an antioxidant defense system in elderly patients with essential hypertension compared with healthy controls. Redox Rep 2011; 16: 71-7.
[30] Qiu X, Brown K, Hirschey MD, Verdin E and Chen D. Calorie restriction reduces oxidative stress by SIRT3-mediated SOD2 activation. Cell Metab 2010; 12: 662-667.
[31] Ionescu-Tucker A and Cotman CW. Emerging roles of oxidative stress in brain aging and Alzheimer's disease. Neurobiol Aging 2021; 107: 86-95.
[32] Zhang M, Su N, Huang Q, Zhang Q, Wang Y, Li J and Ye M. Phosphorylation and antiaging activity of polysaccharide from Trichosanthes peel. J Food Drug Anal 2017; 25: 976-983.
[33] de Los Rios C, Cano-Abad MF, Villarroya M and López MG. Chromaffin cells as a model to evaluate mechanisms of cell death and neuroprotective compounds. Pflugers Arch 2018; 470: 187-198.
[34] Liu YY, Nagpure BV, Wong PT and Bian JS. Hydrogen sulfide protects SH-SY5Y neuronal cells against d-galactose induced cell injury by suppression of advanced glycation end products formation and oxidative stress. Neurochem Int 2013; 62: 603-609.
[35] Ullah F, Ali T, Ullah N and Kim MO. Caffeine prevents d-galactose-induced cognitive deficits, oxidative stress, neuroinflammation and neurodegeneration in the adult rat brain. Neurochem Int 2015; 90: 114-24.
[36] Obeng E. Apoptosis (programmed cell death) and its signals - a review. Braz J Biol 2021; 81: 1133-1143.
[37] Li H, Niu N, Yang J, Dong F, Zhang T, Li S and Zhao W. Nuclear respiratory factor 1 protects H9C2 cells against hypoxia-induced apoptosis via the death receptor pathway and mitochondrial pathway. Cell Biol Int 2021; 45: 1784-1796.
[38] He XY, Chen JL, Xiang H, Gao Y, Tian JS, Qin XM and Du GH. Comparative study of the corticosterone and glutamate induced PC12 cells depression model by 1H NMR metabolomics. Yao Xue Xue Bao 2017; 52: 245-52.
[39] Zhang L, Zhang Y, Ma Z, Zhu Y and Chen Z. Altered amino acid metabolism between coronary heart disease patients with and without type 2 diabetes by quantitative ^{1}H NMR based metabolomics. J Pharm Biomed Anal 2021; 206: 114381.
[40] Song X, Wang X, Liao G, Pan Y, Qian Y and Qiu J. Toxic effects of fipronil and its metabolites on PC12 cell metabolism. Ecotoxicol Environ Saf 2021; 224: 112677.
[41] Nazir N, Zahoor M, Nisar M, Karim N, Latif A, Ahmad S and Uddin Z. Evaluation of neuroprotective and anti-amnesic effects of Elaeagnus umbellata Thunb. On scopolamine-induced memory impairment in mice. BMC Complement Med Ther 2020; 20: 143.
[42] Griffin JW and Bradshaw PC. Amino acid catabolism in Alzheimer's disease brain: friend or foe? Oxid Med Cell Longev 2017; 2017: 5472792.
[43] Santos ALM, Vitório JG, de Paiva MJN, Porto BLS, Guimarães HC, Canuto GAB, Carvalho MDG, de Souza LC, de Toledo JS, Caramelli P, Duarte-Andrade FF and Gomes KB. Frontotemporal dementia: plasma metabolomic signature using gas chromatography-mass spectrometry. J Pharm Biomed Anal 2020; 189: 113424.
[44] Vemula PK, Jing Y, Cicolini J, Zhang H, Mockett BG, Abraham WC and Liu P. Altered brain arginine metabolism with age in the APP_{swe}/$PSEN1_{dE9}$ mouse model of Alzheimer's disease. Neurochem Int 2020; 140: 104798.
[45] Song X, Wang X, Liao G, Pan Y, Qian Y and Qiu J. Toxic effects of fipronil and its metabolites on PC12 cell metabolism. Ecotoxicol Environ Saf 2021; 224: 112677.
[46] Reslane I, Handke LD, Watson GF, Shinde D, Ahn J-S, Endres JL, Razvi F, Gilbert EA, Bayles KW, Thomas VC, Lehman MK and Fey PD. Glutamate-dependent arginine biosynthesis requires the inactivation of *spoVG*, *sarA,* and *ahrC* in *Staphylococcus aureus*. J Bacteriol 2024; 206: e0033723.
[47] Bae YS, Yoon SH, Kim YS, Oh SP, Song WS, Cha JH and Kim MH. Suppression of exaggerated NMDAR activity by memantine treatment ameliorates neurological and behavioral deficits in aminopeptidase P1-deficient mice. Exp Mol Med 2022; 54: 1109-1124.
[48] Khan A and Nayeem SM. Stability of the Aβ42 peptide in mixed solutions of denaturants and proline. J Phys Chem B 2023; 127: 1572-1585.
[49] Kori M, Aydın B, Unal S, Arga KY and Kazan D. Metabolic biomarkers and neurodegeneration: a pathway enrichment analysis of Alzheimer's disease, Parkinson's disease, and amyotrophic lateral sclerosis. OMICS 2016; 20: 645-661.
[50] Sumien N, Shetty RA and Gonzales EB. Creatine, creatine kinase, and aging. Subcell Biochem 2018; 90: 145-168.
[51] Klopstock T, Elstner M and Bender A. Creatine in mouse models of neurodegeneration and aging. Amino Acids 2011; 40: 1297-1303.